

Hole-Burning Spectra of Phenol–Ar_n (*n* = 1, 2) Clusters: Resolution of the Isomer Issue[†]Shun-ichi Ishiuchi,^{‡,§} Yuji Tsuchida,^{‡,§} Otto Dopfer,^{*,‡} Klaus Müller-Dethlefs,^{*,#} and Masaaki Fujii^{*,‡,§,||}

Chemical Resources Laboratory, Tokyo Institute of Technology, 4259 Nagatsuta, Yokohama 226-8503, Japan, Department of Electronic Chemistry, Interdisciplinary Graduate School of Science and Engineering, Tokyo Institute of Technology, 4259 Nagatsuta, Yokohama 226-8502, Japan, Integrated Research Institute, Tokyo Institute of Technology, 4259 Nagatsuta, Yokohama 226-8503, Japan, Institut für Optik und Atomare Physik, Technische Universität Berlin, Hardenbergstrasse 36, D-10623 Berlin, Germany, and The Photon Science Institute, The University of Manchester, Simon Building, Manchester, M13 9PL, United Kingdom

Received: January 30, 2007; In Final Form: March 18, 2007

The hole-burning (HB) spectra of phenol–Ar_n (PhOH–Ar_n) clusters with *n* = 1 and 2 have been measured in a molecular beam to clarify the possible existence of isomers. Two species were identified to give rise to signals in the S₁–S₀ spectrum recorded for the *n* = 1 cluster; however, one of the species was found to originate from dissociation of an *n* = 2 cluster. Similarly, three species were observed in the spectrum of the *n* = 2 cluster, and two of them were assigned to *n* = 3 and larger clusters. The spectral contamination from larger size clusters was quantitatively explained by the dissociation after photoexcitation. The analysis of the spectra demonstrates that only a single isomer exists in the molecular beam for both the *n* = 1 and the *n* = 2 clusters. In addition to two previously detected intermolecular modes, a third low-frequency mode, assigned to an intermolecular bending vibration, is observed for the first time in the HB spectrum of the *n* = 2 cluster. The assignments of the intermolecular vibrations were confirmed by *ab initio* MO calculations. The observation of the third intermolecular vibration suggests that the geometry of the *n* = 2 cluster has C_s or lower symmetry.

1. Introduction

Phenol–Ar_n (PhOH–Ar_n) clusters have been studied to investigate noncovalent interactions since the twilight of supersonic jet laser spectroscopy.¹ PhOH has two major competing intermolecular binding sites: the π -ring that induces a van der Waals bond (π -bound) and the OH group that is a hydrogen-bond active site (H-bound). Therefore, two different types of structures, π -bound and H-bound, can be expected to be global or local minima on the intermolecular potential energy surface. They can be interpreted as hydrophobic and hydrophilic structures, respectively. Thus, the PhOH–Ar_n cluster system constitutes one of the simplest models to learn about the competition of hydrophilic and hydrophobic interactions. Because competition between the hydrophilic and hydrophobic interactions often plays an important role to determine structures of biological supramolecular systems, this benchmark system for hydrophilic/hydrophobic interactions should be characterized and understood in great detail.

In spite of its simplicity, the structures and isomerism of even small-sized PhOH–Ar_n clusters have not been fully determined. In 1985, Gonohe et al. reported resonant-enhanced multiphoton ionization (REMPI) and ionization threshold spectra of PhOH–Ar_n (*n*=1,2) for the first time, and concluded that the π -bound

is favorable in the S₀, S₁, and cationic states.² For the *n* = 2 cluster, a sandwich structure, in which both Ar atoms are located on opposite sides of the benzene ring, was suggested because of the additive red-shifts of the S₁–S₀ transition energy and the ionization potential in terms of the cluster size.² Bieske et al.³ and Mons et al.⁴ assigned the intermolecular vibrations in the REMPI spectrum of PhOH–Ar cluster assuming a π -bound structure. For the PhOH–Ar₂ cluster, Schmidt et al. assigned the intermolecular vibrations on the basis of the sandwich π -bound structure.⁵

The analysis of IR dip^{6,7} and stimulated Raman spectra⁸ also suggests a π -bound structure for PhOH–Ar in S₀ because the OH stretching (ν_{OH}) and skeletal vibrations of bare phenol and PhOH–Ar were observed at almost the same energy. In particular, the frequency of ν_{OH} is a good probe for determining whether a π -bound or an H-bound structure is observed because the latter structure will lead to a red-shift of the vibrational frequency due to the formation of the hydrogen bond.

For the S₁ state, Müller-Dethlefs and co-workers measured the high-resolution REMPI spectrum of PhOH–Ar and concluded the π -bound case based on the rotational contour of the 0–0 transition.⁹ They also measured the pulsed-field-ionization zero-kinetic-energy photoelectron (PFI-ZEKE) and mass-analyzed threshold ionization (MATI) spectra of PhOH–Ar and assigned the intermolecular vibrations in the cationic state assuming a π -bound structure.^{9–12} A π -bound geometry in the cationic state was also supported by the IR spectrum reported by Fujii et al., in which ν_{OH} was observed at 3537 cm⁻¹, in coincidence with ν_{OH} of bare phenol.^{13–15}

So far, the PhOH–Ar cluster had been believed to possess a π -bound structure in the S₀, S₁, and cationic states. However, this general belief was reversed in 2000 by Dopfer and

[†] Part of the “Roger E. Miller Memorial Issue”.

* Corresponding authors. E-mail mfujii@res.titech.ac.jp; (M.F.); dopfer@physik.tu-berlin.de (O.D.); k.muller-dethlefs@manchester.ac.uk (K.M.-D.).

[‡] Chemical Resources Laboratory, Tokyo Institute of Technology.

[§] Department of Electronic Chemistry, Interdisciplinary Graduate School of Science and Engineering, Tokyo Institute of Technology.

^{||} Integrated Research Institute, Tokyo Institute of Technology.

[‡] Institut für Optik und Atomare Physik, Technische Universität Berlin.

[#] The Photon Science Institute, Simon Building, The University of Manchester.

co-workers.^{16–20} They measured the IR spectrum of the PhOH–Ar cluster cation produced by electron impact ionization and observed an intense band at 3464 cm^{-1} , which is clearly red-shifted from the free OH stretching vibration (3537 cm^{-1}) observed for the PhOH–Ar cation produced by photoionization. This red-shifted band was assigned to the ν_{OH} mode of the OH \cdots Ar configuration, which means that the H-bound structure is the most stable geometry in the cationic state. This observation is fully supported by ab initio MO calculations. The disagreement between the PhOH–Ar cation structures observed by photoionization (π -bond) and electron impact ionization (H-bond) can be explained by the differences in the ionization processes. Photoionization induces a vertical transition according to the Franck–Condon principle, and the structure of the cluster is maintained after ionization. Thus, the π -bound cation arises from ionization of the π -bound S_0 state via the $(1 + 1')$ REMPI process, although it is a less stable conformation. On the other hand, cluster generation by electron impact ionization does not have such a restriction, and the most stable H-bound structure is produced.^{18,20}

If the ionization excess energy is increased, the π -bound cluster cation (local minimum) produced by photoionization might undergo an isomerization reaction toward the H-bound global minimum. Recently, we detected such an isomerization reaction in the PhOH–Ar₂ cation produced by $(1 + 1')$ REMPI.²¹ We applied picosecond time-resolved UV–UV–IR dip spectroscopy to the PhOH–Ar₂ cluster and measured the picosecond time-resolved vibrational spectra in the OH stretching region. Just after ionization, only the free ν_{OH} (3537 cm^{-1}) of the π -bound structure was observed, while another red-shifted ν_{OH} (3464 cm^{-1}), which derives from the H-bound structure, appeared a few picoseconds later. At about 10 ps after ionization, the π -bound ν_{OH} disappeared, and only the H-bound ν_{OH} was observed. This result implies that the $\pi \rightarrow$ H isomerization reaction occurs in the PhOH–Ar₂ cation with 100% yield. In addition, this reaction was observed even when the cluster cation was produced at the adiabatic ionization potential, where the cluster cation was generated in the vibrational ground state. Apparently, $\pi \rightarrow$ H isomerization in the PhOH–Ar₂ cluster cation has no barrier.

In summary, very recent spectroscopic experiments for PhOH–Ar_n clusters identified H-bound global minima ($n = 1–5$)¹⁸ and a $\pi \rightarrow$ H isomerization process ($n = 2$) in the cationic state,²¹ although the H-bound conformation was not positively expected before. Under these circumstances, the structures and isomerism of PhOH–Ar_n clusters should also be re-examined for the neutral ground state. So far, only the π -bound structure has been observed. However, an extensive survey as to whether other isomers coexist, such as measuring hole-burning spectra, has not yet been carried out. In this paper, we report on the hole-burning spectra of PhOH–Ar_n clusters and discuss whether any isomers coexist or not. In addition, the assignments of the intermolecular vibrations are discussed because weak vibronic bands can be detected by hole-burning spectroscopy.

2. Experimental

Figure 1 shows the principle of hole-burning (HB) spectroscopy.^{22–27} A probe laser, ν_{P} , is fixed to the S_1 – S_0 transition of the considered PhOH–Ar_n cluster. The electronically excited PhOH–Ar_n cluster is then ionized by an ionization laser, ν_{ION} , which excites the cluster to a slightly higher energy than its ionization potential in order to avoid dissociation of the clusters (soft ionization). The ion current of PhOH⁺–Ar_n created by ν_{P}

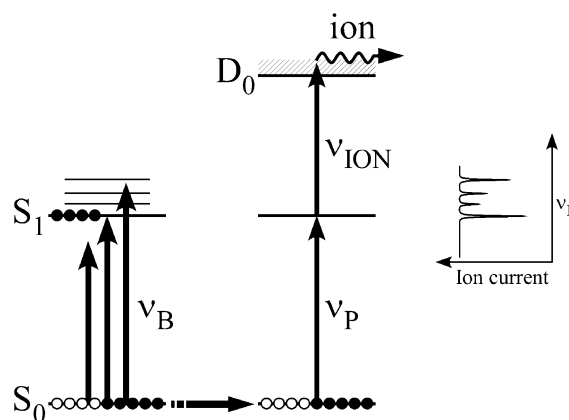


Figure 1. Principle of hole-burning (HB) spectroscopy.

and ν_{ION} is proportional to the population of the zero vibrational level of PhOH–Ar_n in the S_0 state. Prior to ν_{P} , an intense burn laser, ν_{B} , is fired and scanned. If ν_{B} is resonant to one of the S_1 – S_0 transitions of PhOH–Ar_n, and the cluster is electronically excited, the ion current of PhOH⁺–Ar_n decreases. Thus, by scanning ν_{B} while monitoring the ion current of PhOH⁺–Ar_n arising from ν_{P} and ν_{ION} , the electronic spectrum of a single specific species can be measured.

The probe laser, ν_{P} , and the burn laser, ν_{B} , were obtained by frequency-doubled dye lasers (Lumonics HD-500; Sirah Cobra-Stretch), which were pumped by the third harmonics of Nd³⁺:YAG lasers (Spectra Physics GCR-170, INDI-40). The ionization laser, ν_{ION} , was obtained by a frequency-doubled dye laser (Lumonics HD-500), which was pumped by the second harmonic of a Nd³⁺:YAG laser (Continuum Powerlite-8010). By a beam combiner, ν_{P} and ν_{ION} were aligned coaxially and were introduced to a vacuum chamber from the opposite direction to ν_{B} . The probe laser, ν_{P} , and the ionization laser, ν_{ION} , were fired simultaneously about 2 μs after ν_{B} .

Phenol (Sigma Aldrich, 99% purity), which was purified by vacuum sublimation, was evaporated at 40 °C and expanded with Ar (4 bar) into the vacuum chamber through a pulsed valve (General Valve, series 9). A molecular beam was introduced through a skimmer (dim. 2 mm) into an ionization chamber, where it was intersected with the three laser beams, ν_{B} , ν_{P} , and ν_{ION} . The generated cations were extracted into a time-of-flight mass spectrometer by a repeller electrode and detected by a homemade Even-cup detector.²⁸ Because the intense burn laser ν_{B} produced abundant cations, the ion bunch created by ν_{B} was removed by a pulsed deflector in order to avoid saturation of the ion detector.

The probe laser, ν_{P} , and the ionization laser, ν_{ION} , were operated at 20 Hz, while the burn laser, ν_{B} , was operated at 10 Hz. Thus, we could obtain a $\nu_{\text{B}} + \nu_{\text{P}} + \nu_{\text{ION}}$ signal and a $\nu_{\text{P}} + \nu_{\text{ION}}$ signal alternatively. These two signals were separately integrated and stored in a digital boxcar system (EG&G PARC 4420/4422) after amplification by a preamplifier (NF BX-31A).²⁹ The integrated signals were recorded by a personal computer. Fluctuations in the conditions of the pulsed valve were suppressed by calculating the ratio between the two signals.

3. Results and Discussion

A. HB Spectrum of the PhOH–Ar ($n = 1$) Cluster. Figure 2a shows the $(1 + 1')$ REMPI spectrum of the PhOH–Ar ($n=1$) cluster using $\nu_{\text{ION}} = 32\,258\text{ cm}^{-1}$. The most intense band at $36\,316\text{ cm}^{-1}$ is assigned to the 0–0 transition of π -bound PhOH–Ar.^{2–4,10} The same REMPI spectrum is also reproduced with $5\times$ magnification along the vertical axis to show weak

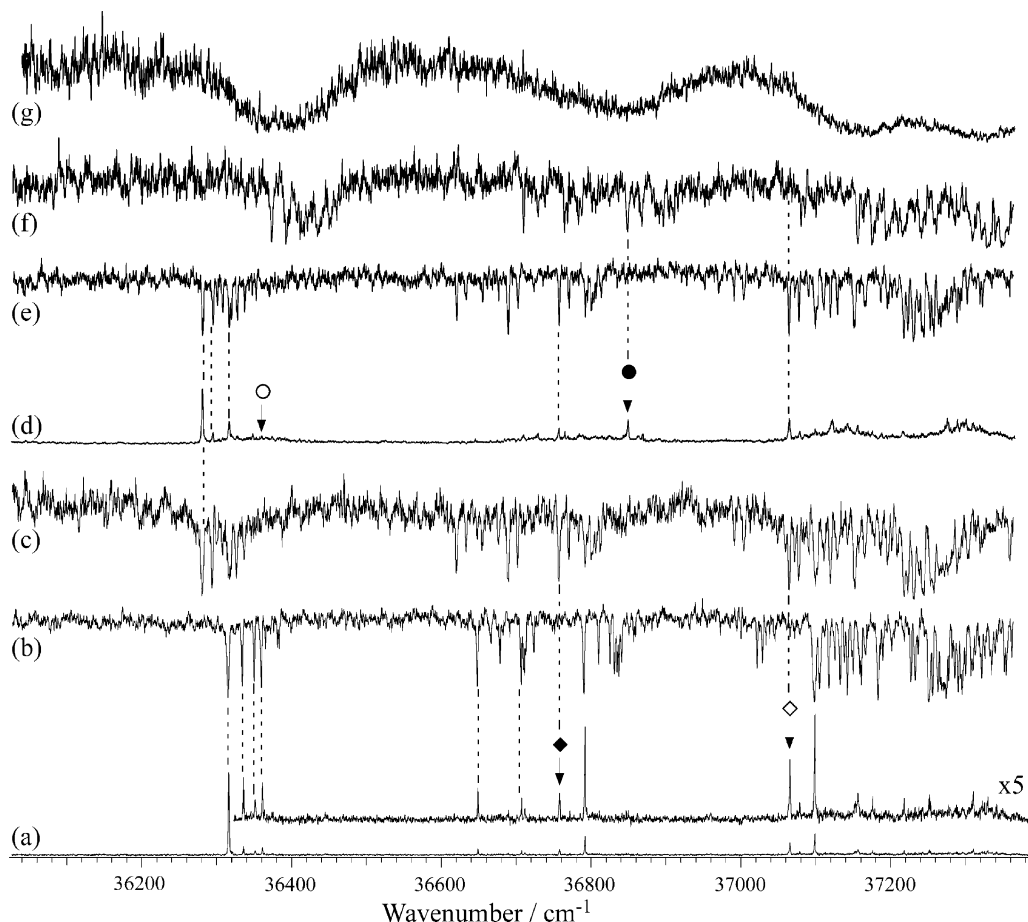


Figure 2. (a) REMPI spectrum measured by monitoring the mass peak of PhOH-Ar. (b,c) HB spectra measured by monitoring the mass peak of PhOH-Ar and fixing the probe laser, ν_p , to 36 316 and 36 758 cm^{-1} , respectively. (d) REMPI spectrum measured by monitoring the mass peak of PhOH-Ar₂. (e-g) HB spectra measured by monitoring the mass peak of PhOH-Ar₂ and fixing the probe laser, ν_p , to 36 281, 36 850, and 36 360 cm^{-1} , respectively.

low-frequency bands. Figure 2b displays the HB spectrum recorded for $\nu_p = 36\,316\text{ cm}^{-1}$. Because of the intense burn laser, ν_B , we successfully observed many weak bands in the HB spectrum. By comparing these spectra, it was found that almost all of the bands observed in the REMPI spectrum appear in the HB spectrum, except for bands at 36 758 and 37 066 cm^{-1} , which are indicated by \blacklozenge and \blacklozenge , respectively. The HB spectrum measured by fixing ν_p to 36 758 cm^{-1} is shown in Figure 2c. At a glance, it can be found that the two HB spectra shown in parts b and c of Figure 2 are completely different. Thus, it is concluded that the electronic transition observed at 36 758 cm^{-1} derives from a species other than π -bound PhOH-Ar, of which the 0-0 transition is located at 36 316 cm^{-1} . The band at 37 066 cm^{-1} was also observed in the HB spectrum in Figure 2c. This observation implies that the electronic transitions at 36 316 and 37 066 cm^{-1} originate from the same species. Thus, we observed in total two different species in the REMPI spectrum in Figure 2a, monitoring the PhOH-Ar mass channel.

In the region below 36 758 cm^{-1} , the new species shows several intense bands comparable to the bands at 36 758 cm^{-1} (\blacklozenge) or 37 066 cm^{-1} (\blacklozenge) in the HB spectrum. However, these bands do not appear in the REMPI spectrum at all. In addition, a band observed at 36 281 cm^{-1} in the HB spectrum, which seems to be a 0-0 transition of the new species, coincides with the 0-0 transition of the PhOH-Ar₂ cluster ($n = 2$). According to these results, it is a natural interpretation that the new species observed in the HB spectrum in Figure 2c is not a second isomer of the PhOH-Ar cluster ($n = 1$), but a PhOH-Ar cluster

produced by evaporation of one Ar atom from the PhOH-Ar₂ cluster ($n = 2$).

This interpretation is confirmed by measuring the HB spectrum of the PhOH-Ar₂ cluster (Figure 2e). Also, the mass-selected REMPI spectrum of the PhOH-Ar₂ cluster is shown in Figure 2d. For the HB spectrum 2e, the probe laser, ν_p , was fixed to the 0-0 transition of PhOH-Ar₂ (36 281 cm^{-1}), whereas the ionization laser, ν_{ION} , was fixed to 31 889 cm^{-1} . By comparing the two HB spectra in parts c and e of Figure 2, it is easily found that both spectra are the same. Thus, the bands observed at 36 316 and 37 066 cm^{-1} in the mass-selected REMPI spectrum of the PhOH-Ar cluster ($n = 1$) derive not from an isomer of PhOH-Ar, such as the H-bound isomer, but from Ar fragmentation of the PhOH-Ar₂ cluster ($n = 2$). Therefore, it is concluded that the PhOH-Ar dimer occurs as a single isomer in the molecular beam expansion. The energetics of the dissociation process of PhOH-Ar₂ is discussed below.

B. HB Spectrum of the PhOH-Ar₂ ($n = 2$) Cluster.

Similarly to the PhOH-Ar ($n = 1$) cluster, we examined the existence of isomers for the PhOH-Ar₂ ($n = 2$) cluster by comparing the REMPI spectrum^{2,5,10} of PhOH-Ar₂ (Figure 2d) with the HB spectrum (Figure 2e) in detail. The bands observed in the REMPI spectrum also appear in the HB spectrum, except for those at 36 710, 36 729, and 36 850 cm^{-1} . Thus, the species that give rise to these electronic transitions are different from those of the π -bound PhOH-Ar₂ cluster. To confirm this result, we measured the HB spectrum by fixing ν_p to 36 850 cm^{-1} , represented by \bullet . In the resulting HB spectrum (Figure 2f), the bands observed at 36 710 and 36 729 cm^{-1} in the REMPI

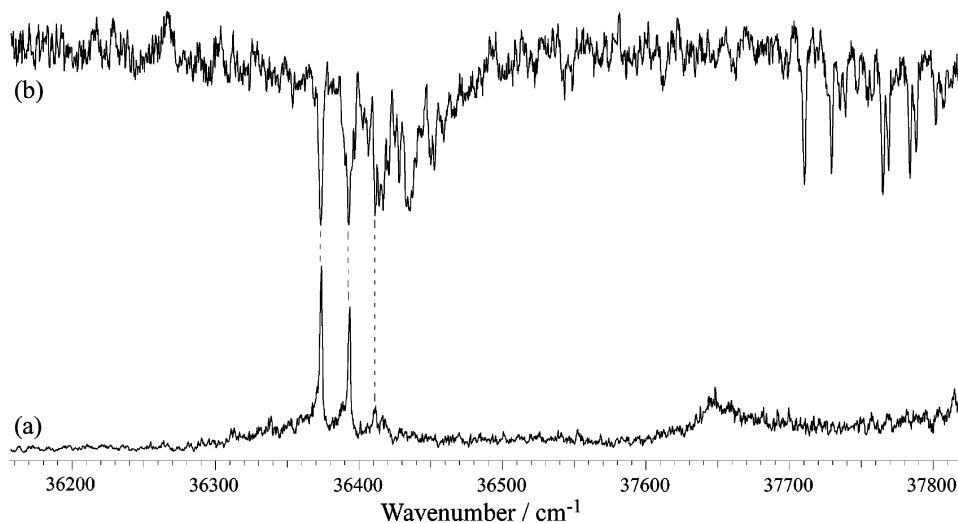


Figure 3. (a) REMPI spectrum measured by monitoring the mass peak of PhOH-Ar_3 . (b) HB spectrum measured by monitoring the mass peak of PhOH-Ar_3 and fixing the probe laser, ν_p , to $36\,373\text{ cm}^{-1}$, which is the 0–0 transition of PhOH-Ar_3 .

spectrum (Figure 2d) were also observed. Thus, these bands originate from the same species, giving rise to the electronic transition at $36\,850\text{ cm}^{-1}$.

The bands detected below $36\,710\text{ cm}^{-1}$ in the HB spectrum did not appear in the REMPI spectrum. Furthermore, the transition observed at $36\,373\text{ cm}^{-1}$ in the HB spectrum coincides with the 0–0 transition of the PhOH-Ar_3 cluster ($n = 3$).¹⁰ Similarly to the HB spectrum of PhOH-Ar , this observation suggests that the carrier of this transition can also be expected to be generated by the evaporation of one Ar ligand from PhOH-Ar_3 . Figure 3 shows the mass-selected REMPI spectrum (a) and the HB spectrum (b) obtained by fixing ν_p to the 0–0 band of PhOH-Ar_3 . From these spectra, it is concluded that the sharp bands observed at $36\,710$, $36\,729$, and $36\,850\text{ cm}^{-1}$ in the REMPI spectrum in Figure 2d can be assigned to the electronic transitions of the PhOH-Ar_3 cluster, which contaminates the spectrum of PhOH-Ar_2 due to the evaporation of one Ar atom.

In addition, a broad background observed under sharp peaks in the REMPI spectrum (Figure 2d) is not observed in the HB spectrum (Figure 2e). For example, the broad band with a maximum at $36\,360\text{ cm}^{-1}$ can be seen in the mass-selected REMPI spectrum (Figure 2d). However, its correspondence to the HB spectrum is not clear. To clarify the correspondence, the HB spectrum was measured by fixing ν_p to the maximum of the broad signal represented by \circ . The resulting HB spectrum is shown in Figure 2g. The spectral feature is clearly different from the REMPI spectrum in Figure 2d, and only broad bands are observed. Therefore, the broad background observed in the REMPI spectrum in Figure 2d originates from the same species, which is different from the π -bound PhOH-Ar_2 cluster and the PhOH-Ar_3 cluster. We tentatively attribute this species to larger PhOH-Ar_n clusters with $n > 3$, which give rise to the signal in the PhOH-Ar_2 mass channel by the evaporation of Ar atoms.

In summary, we have concluded that only a single isomeric PhOH-Ar_2 species is observed in the REMPI spectrum of the PhOH-Ar_2 cluster. Thus, similarly to the PhOH-Ar dimer, the PhOH-Ar_2 trimer occurs as a single isomer in the molecular beam expansion.

C. Dissociation Process of the PhOH-Ar_2 ($n = 2$) Cluster.

The absence of the PhOH-Ar_2 bands below $36\,758\text{ cm}^{-1}$ in the REMPI spectrum of PhOH-Ar (Figure 2a) originating from the dissociation of PhOH-Ar_2 can be explained by the

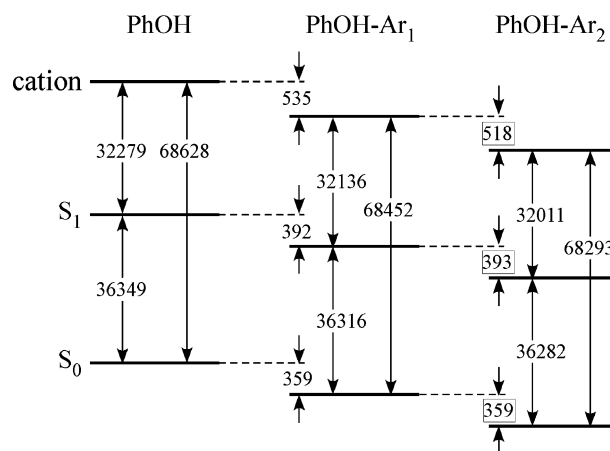


Figure 4. Energy diagram (cm^{-1}) of electronic transitions of PhOH-Ar_n ($n = 0-2$). The values in boxes were obtained based on the assumption that the dissociation energy of $\text{PhOH-Ar}_2 \rightarrow \text{PhOH-Ar} + \text{Ar}$ equals that of $\text{PhOH-Ar} \rightarrow \text{PhOH} + \text{Ar}$ in the S_0 state.

dissociation energy of the Ar atom. The dissociation energy of the π -bound PhOH-Ar cation has already been measured by Müller-Dethlefs and co-workers via MATI spectroscopy and was reported to be $535 \pm 3\text{ cm}^{-1}$.^{11,12} On the basis of this value, S_1-S_0 transition energies, and ionization potentials of the PhOH monomer and the PhOH-Ar cluster, we can obtain the dissociation energies in the S_1 and S_0 state, which are summarized in Figure 4. The dissociation energy of the PhOH-Ar_2 cluster cation has not been measured. We assumed that the dissociation energy of the PhOH-Ar_2 cluster in the S_0 state is the same as that of the PhOH-Ar cluster in S_0 , because both clusters have a π -bound structure, and the Ar–Ar interaction in the PhOH-Ar_2 cluster is expected to be weak in the neutral. According to this assumption, we estimated the dissociation energies of the PhOH-Ar_2 cluster in the S_1 and cationic states. The estimated dissociation energy of the PhOH-Ar_2 cluster in the S_1 state is almost the same as that of PhOH-Ar ($n = 1$) cluster in S_1 , which supports our assumption.

For measurements of the $1 + 1'$ REMPI spectrum, PhOH-Ar_n clusters can dissociate in both the S_1 state and the cationic state. When the REMPI spectrum of the PhOH-Ar cluster ($n = 1$) is measured, the electronically excited PhOH-Ar_2 cluster ($n = 2$) can dissociate into PhOH-Ar in the S_1 state if ν_p has a higher energy than $36\,675$ ($36\,282 + 393$) cm^{-1} (Figure 4). In the cationic state, the PhOH-Ar_2 cluster cation can dissociate

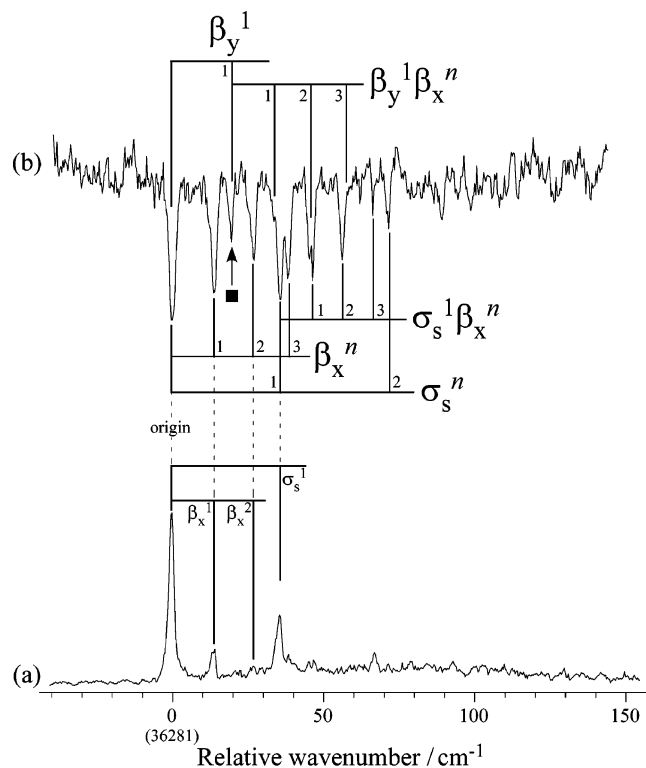


Figure 5. REMPI spectrum (a) and HB spectrum (b) of PhOH–Ar₂ in the vicinity of the electronic S₁ origin.

into the PhOH–Ar cluster cation if ν_P has an energy higher than 36 553 (68 293 + 518 – 32 258 (ν_{ION})) cm⁻¹. In the REMPI spectrum of PhOH–Ar (Figure 2a), no bands are observed below 36 758 cm⁻¹. Therefore, the dissociation processes in both the S₁ and cationic state can energetically explain this threshold consistently.

D. Intermolecular Vibrations of the PhOH–Ar₂ (n = 2) Cluster. As mentioned in the Introduction, the PhOH–Ar₂ cluster (n = 2) exhibits the $\pi \rightarrow \text{H}$ site-switching dynamics induced by photoionization.²¹ This isomerization reaction is not observed for the PhOH–Ar dimer (n = 1). To understand why the isomerization reaction does not occur for PhOH–Ar but for PhOH–Ar₂, reliable information about the accurate geometry of PhOH–Ar₂ is required. According to our previous studies by picosecond IR spectroscopy, we concluded that the PhOH–Ar₂ cluster in S₀ has no H-bound ligand.²¹ However, we could not conclude about the specific position of both π -bound ligands, that is, whether both Ar atoms are located on opposite sides of the benzene ring, represented by (1|1), or whether they are both binding on the same side, represented by (2|0), respectively. Both isomeric structures were observed for benzene–Ar₂.³⁰ In previous studies described in the Introduction, the PhOH–Ar₂ cluster was suggested to have the (1|1) structure based on the additive red-shifts both in the S₁–S₀ transition energy and the ionization potential with increasing cluster size (for n = 0–2). Such an additive red-shift is not observed for the benzene–Ar₂ (2|0) isomer. However, the (2|0) structure may explain the different reactivity between the n = 1 and n = 2 clusters for $\pi \rightarrow \text{H}$ site switching of PhOH–Ar_n. Here, we tried to derive any evidence for the geometry of PhOH–Ar₂ from the intermolecular vibrations, which were sensitively observed by HB spectroscopy.

Figure 5 shows (a) the REMPI spectrum and (b) the HB spectrum of PhOH–Ar₂ in the vicinity of the S₁ origin. In the REMPI spectrum, two progressions were observed. The assignments reported by Schmidt et al. are indicated in Figure 5a.⁵

The assignments by Haines et al. are also shown in the lower part of Figure 5b.¹⁰ The vibrational motions of the six possible intermolecular modes of the (1|1) and (2|0) structures are depicted in Figure 6. Here, the in-phase and out-of-phase intermolecular stretching modes are represented by σ_s and σ_a , respectively. The in-phase and out-of-phase sliding modes along the x-axis and the y-axis are represented by β_x , β_y and λ_x , λ_y , respectively. The symmetry of each mode in the C_s point group is also indicated in the figure, together with the symmetry correlated with the C_{2v} point group (in parentheses). In previous assignments, the symmetry of the normal modes of the (1|1) structure was evaluated in the C_{2v} point group, that is, the OH group was regarded as an atom. This assumption was used to explain why only progressions involving two intermolecular modes are observed.⁵ In the C_{2v} point group, only two intermolecular vibrational modes (σ_s and β_x) are totally symmetric (a₁) and can be observed without vibronic coupling. On the other hand, because the proper C_s point group has three totally symmetric a' modes (σ_s , β_x , and β_y), the (1|1) structure could display three intense vibrational modes in the electronically allowed S₁–S₀ transition. Because the (2|0) structure belongs to the C₁ point group, all the intermolecular vibrations are allowed for this isomer. Schmidt et al. argued that the appearance of two intermolecular vibrational modes in the REMPI spectrum is indicative of C_{2v} symmetry and assigned the intermolecular modes as σ_s and β_x based on a consideration of the respective reduced masses.⁵

Let us discuss now the assignments of the intermolecular bands observed in the HB spectrum of PhOH–Ar₂. According to the previous assignments,^{5,10} the transitions at 0° + 14 cm⁻¹ and 0° + 27 cm⁻¹ are assigned to β_x^1 and β_x^2 , respectively. The intense band at 0° + 36 cm⁻¹ is attributed to σ_s^1 . Almost all of the bands observed in the HB spectrum can be assigned by progressions and combinations of σ_s and β_x , except for a band at 0° + 20 cm⁻¹, represented by ■, which is not observed in the REMPI spectrum.^{5,10} The absence of this band in the REMPI spectrum is probably because of its weakness. In the HB spectrum, weak transitions are enhanced owing to saturation effects. Consequently, the HB spectrum provides more spectral information compared to the REMPI spectrum. As mentioned above, β_y is forbidden in the C_{2v} approximation but is allowed in C_s symmetry. Therefore, the transition strength for β_y is expected to be weaker than those of σ_s and β_x . Thus, we assign the band at 0° + 20 cm⁻¹ to β_y^1 . This mode occurs also in combination with a progression in β_x . On the basis of σ_s , β_x , and β_y , we can assign all of the low-frequency bands in the HB spectrum of PhOH–Ar₂. The intermolecular vibrations accompanying other skeletal vibrations of the phenol chromophore were also assigned. The observed vibrational frequencies and assignments are listed in Table 1. The intermolecular vibration β_y could not be detected for the region of the skeletal vibrations. The skeletal vibrations are weaker than the origin, thus the absence of the combination vibration between the skeletal and β_y vibrations is due to its weakness.

To support the assignments, the vibrational frequencies of the intermolecular modes in S₀ of PhOH–Ar₂ were also determined by ab initio MO calculations at the MP2/6-311++G(d,p) level using the Gaussian03 program.³¹ The calculated frequencies for the (1|1) and (2|0) isomers are listed in Table 2, together with the frequencies observed in S₁. The order of the vibrational frequencies is well reproduced by both the (1|1) and the (2|0) isomers. The good reproduction of the experimental frequencies measured in S₁ by the calculated frequencies in S₀ suggests that the geometry and interaction

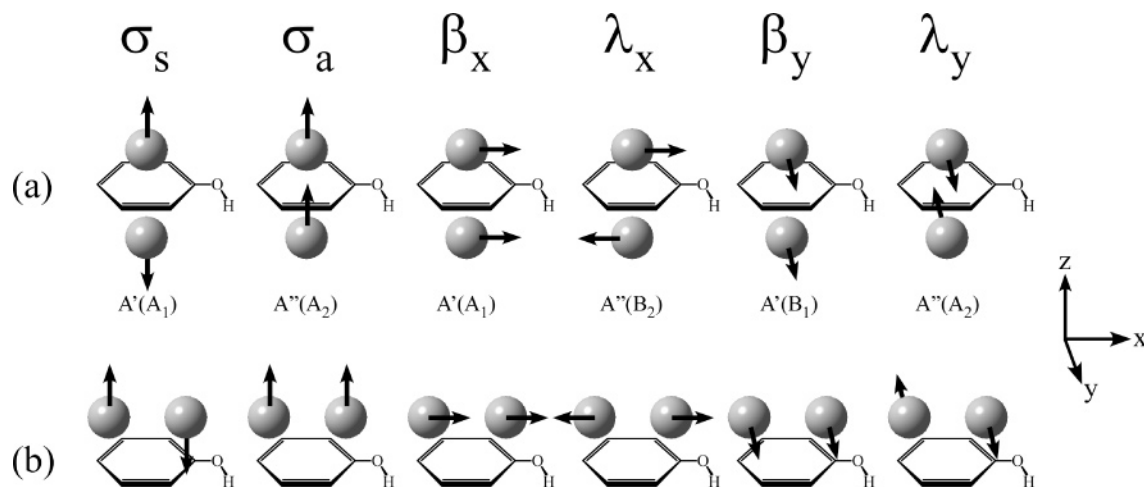


Figure 6. Intermolecular vibrational motions of (a) the (1|1) structure and (b) the (2|0) structure of PhOH–Ar₂. The symmetries of the vibrational motions of (1|1) are classified by the C_s and C_{2v} (in parentheses) point groups.

TABLE 1: Assignments of the Observed Bands (cm^{-1}) in the HB Spectrum of PhOH–Ar₂

frequency	assignment	frequency	assignment	frequency	assignment
0 (36281)	0^0	476	$6a^1$	914	$16b^2\sigma_s^1\beta_x^1$
14	β_x^1	489	$6a^1\beta_x^1$	936	1^1
20	β_y^1	511	$6a^1\sigma_s^1$	942	$6a^2$
27	β_x^2	514	$6a^1\beta_x^3$	949	$1^1\beta_x^1$
33	$\beta_x^1\beta_y^1$	521	$6a^1\sigma_s^1\beta_x^1$	957	$6a^2\beta_x^1$
36	σ_s^1	532	$6a^1\sigma_s^1\beta_x^2$	963	$1^1\beta_x^2$
39	β_x^3	710	$10b^11^1$	972	$1^1\sigma_s^1$
46	$\beta_x^2\beta_y^1$	723	$10b^11^1\beta_x^1$	976	$6a^2\sigma_s^1$
47	$\sigma_s^1\beta_x^1$	783	12^1	983	$1^1\sigma_s^1\beta_x^1$
57	$\sigma_s^1\beta_x^2$	797	$12^1\beta_x^1$	986	$6a^2\sigma_s^1\beta_x^1$
67	$\sigma_s^1\beta_x^3$	809	$12^1\beta_x^2$	996	$1^1\sigma_s^1\beta_x^2$
72	σ_s^2	818	$12^1\sigma_s^1$	1007	β_{OH}^1
339	11^2	829	$12^1\beta_x^2\beta_y^1$	1021	$\beta_{\text{OH}}^1\beta_x^1$
352	$11^2\beta_x^1$	830	$12^1\sigma_s^1\beta_x^1$	1037	$\beta_{\text{OH}}^1\beta_x^2$
373	$11^2\sigma_s^1$	838	$12^1\sigma_s^1\beta_x^2$	1041	$\beta_{\text{OH}}^1\sigma_s^1$
395	$11^2\sigma_s^1\beta_x^2$	848	$12^1\sigma_s^1\beta_x^3$	1054	$\beta_{\text{OH}}^1\sigma_s^1\beta_x^1$
408	$11^2\sigma_s^1\beta_x^3$	870	$16b^2$	1078	$\beta_{\text{OH}}^1\sigma_s^2$
413	$11^2\sigma_s^2$	884	$16b^2\beta_x^1$		
420	$11^2\sigma_s^1\beta_x^4$	906	$16b^2\sigma_s^1$		

TABLE 2: Observed Frequencies (cm^{-1}) in the HB Spectrum of PhOH–Ar₂ Cluster and Frequencies Calculated for the (1|1) and (2|0) Structures

mode	expt	calcd (1 1)	calcd (2 0)
σ_s	36	45	60
σ_a		67	54
β_x	14	17	9.9
λ_x		37	33
β_y	20	19	30
λ_y		61	6.1

energy of the cluster is not changed much upon photoexcitation. This conclusion is consistent with the observation that the S_1 origin is the strongest band in the REMPI spectrum and that the observed intermolecular progressions are short.

The appearance of the third intermolecular vibrational mode clearly suggests that the geometry of the PhOH–Ar₂ cluster has C_s or lower symmetry (neglecting effects of vibronic coupling), which is compatible with both the (1|1) and the (2|0) isomer, respectively. We tried to find a fourth intermolecular vibrational mode because the appearance of such a fourth vibrational mode would be positive evidence of C_1 symmetry, which is only consistent with the (2|0) structure. However, such a low-frequency band was not assignable. As described in the Introduction, the additive red-shift is indicative of the (1|1) structure. However, it is also true that no logical and definitive evidence to exclude the (2|0) structure has been obtained until

the present time. High-level quantum chemical calculation and/or high-resolution spectroscopy should be applied to unambiguously determine the geometry of the PhOH–Ar₂ cluster.

4. Conclusion

We have measured and analyzed the hole-burning (HB) spectra of PhOH–Ar and PhOH–Ar₂ to investigate whether several isomers of these clusters coexist in a molecular beam expansion. Two species have been identified in the HB spectra of PhOH–Ar, however, one was found to originate from fragmentation of PhOH–Ar₂. Similarly, three species were observed in the HB spectra of PhOH–Ar₂, and two of them were found to stem from dissociation of PhOH–Ar_n with $n \geq 3$. Thus, we concluded that PhOH–Ar and PhOH–Ar₂ occur as single π -bound isomers in the molecular beam expansion. On the basis of the binding energy of π -bound PhOH–Ar, the energetics of the dissociation processes observed for both PhOH–Ar and PhOH–Ar₂ are consistent with fragmentation occurring in the S_1 and/or cationic state.

In the HB spectrum of PhOH–Ar₂, we observed many intermolecular vibrations sensitively and found a new band. We assigned this newly observed transition to the second intermolecular bending mode, β_y^1 . This observation means that the structure of the PhOH–Ar₂ cluster has C_s or lower symmetry, which is consistent with the previously suggested (1|1) structure. However, this result does not exclude, in principle, the (2|0) structure. To definitively determine the geometry of PhOH–Ar₂, high-resolution spectra and high-level quantum chemical calculations will be carried out in the near future.

Acknowledgment. The present work was financially supported in part by a Grant-in-Aid from the Ministry of Education, Culture, Sports, Science and Technology (MEXT). O.D. and M.F. thank the Japan Society for Promotion of Science for support of the international collaboration. K.M.-D. gratefully acknowledges support from the Royal Society for a joint UK–Japan research project.

References and Notes

- (1) Gough, T. E.; Miller, R. E.; Scoles, G. *Appl. Phys. Lett.* **1977**, *30*, 338.
- (2) Gonohe, N.; Abe, H.; Mikami, N.; Ito, M. *J. Phys. Chem.* **1985**, *89*, 3642.
- (3) Bieske, E. J.; Rainbird, M. W.; Atkinson, I. M.; Knight, A. E. W. *J. Chem. Phys.* **1989**, *91*, 752.

- (4) Mons, M.; Calvé, J. L.; Piuze, F.; Dimicoli, I. *J. Chem. Phys.* **1990**, *92*, 2155.
- (5) Schmidt, M.; Mons, M.; Calvé, J. L. *Z. Phys. D* **1990**, *17*, 153.
- (6) Fujii, A.; Miyazaki, M.; Ebata, T.; Mikami, N. *J. Chem. Phys.* **1999**, *110*, 11125.
- (7) Ebata, T.; Iwasaki, A.; Mikami, N. *J. Phys. Chem. A* **2000**, *104*, 7974.
- (8) Hartland, G. V.; Henson, B. F.; Venturo, V. A.; Felker, P. M. *J. Phys. Chem.* **1992**, *96*, 1164.
- (9) Ford, M. S.; Haines, S. R.; Pugliesi, I.; Dessent, C. E. H.; Müller-Dethlefs, K. *J. Electron Spectrosc.* **2000**, *112*, 231.
- (10) Haines, S. R.; Dessent, C. E. H.; Müller-Dethlefs, K. *J. Electron Spectrosc.* **2000**, *108*, 1.
- (11) Dessent, C. E. H.; Müller-Dethlefs, K. *Chem. Rev.* **2000**, *100*, 3999.
- (12) Dessent, C. E. H.; Haines, S. R.; Müller-Dethlefs, K. *Chem. Phys. Lett.* **1999**, *315*, 103.
- (13) Fujii, A.; Sawamura, T.; Tanabe, S.; Ebata, T.; Mikami, N. *Chem. Phys. Lett.* **1994**, *225*, 104.
- (14) Fujii, A.; Iwasaki, A.; Ebata, T.; Mikami, N. *J. Phys. Chem. A* **1997**, *101*, 5963.
- (15) Ebata, T.; Fujii, A.; Mikami, N. *Int. Rev. Phys. Chem.* **1998**, *17*, 331.
- (16) Solcá, N.; Dopfer, O. *Chem. Phys. Lett.* **2000**, *325*, 354.
- (17) Solcá, N.; Dopfer, O. *J. Mol. Struct.* **2001**, *563*, 241.
- (18) Solcá, N.; Dopfer, O. *J. Phys. Chem. A* **2001**, *105*, 5637.
- (19) Solcá, N.; Dopfer, O. *Chem. Phys. Lett.* **2003**, *369*, 68.
- (20) Dopfer, O. *Z. Phys. Chem.* **2005**, *219*, 125.
- (21) Ishiuchi, S.; Sakai, M.; Tsuchida, Y.; Takeda, A.; Kawashima, Y.; Fujii, M.; Dopfer, O.; Müller-Dethlefs, K. *Angew. Chem., Int. Ed.* **2005**, *44*, 6149.
- (22) Lipert, R. J.; Colson, S. D. *J. Phys. Chem.* **1989**, *93*, 3894.
- (23) Lipert, R. J.; Colson, S. D. *Chem. Phys. Lett.* **1989**, *161*, 303.
- (24) Pohl, M.; Schmitt, M.; Kleinermanns, K. *Chem. Phys. Lett.* **1991**, *177*, 252.
- (25) Schmitt, M.; Müller, H.; Kleinermanns, K. *Chem. Phys. Lett.* **1994**, *218*, 246.
- (26) Schmitt, M.; Henrich, U.; Müller, H.; Kleinermanns, K. *J. Chem. Phys.* **1995**, *103*, 918.
- (27) Ebata, T. *Nonlinear Spectroscopy for Molecular Structure Determination*; Field, R. W., Hirota, E., Maier, J. P., Tsuchiya, S., Eds.; Blackwell Science; Cambridge, MA, 1998; Chapter 6 Population Labeling Spectroscopy, pp 149–165.
- (28) Bahat, D.; Cheshnovsky, O.; Even, U.; Lavie, N.; Magen, Y. *J. Phys. Chem.* **1987**, *91*, 2460.
- (29) Okuzawa, Y.; Fujii, M.; Ito, M. *Chem. Phys. Lett.* **1990**, *171*, 341.
- (30) Schmidt, M.; Mons, M.; Calvé, J. L. *Chem. Phys. Lett.* **1991**, *177*, 371.
- (31) Frisch, M. J.; Trucks, G. W.; Schlegel, H. B.; Scuseria, G. E.; Robb, M. A.; Cheeseman, J. R.; Montgomery, J. A., Jr.; Vreven, T.; Kudin, K. N.; Burant, J. C.; Millam, J. M.; Iyengar, S. S.; Tomasi, J.; Barone, V.; Mennucci, B.; Cossi, M.; Scalmani, G.; Rega, N.; Petersson, G. A.; Nakatsuji, H.; Hada, M.; Ehara, M.; Toyota, K.; Fukuda, R.; Hasegawa, J.; Ishida, M.; Nakajima, T.; Honda, Y.; Kitao, O.; Nakai, H.; Klene, M.; Li, X.; Knox, J. E.; Hratchian, H. P.; Cross, J. B.; Bakken, V.; Adamo, C.; Jaramillo, J.; Gomperts, R.; Stratmann, R. E.; Yazyev, O.; Austin, A. J.; Cammi, R.; Pomelli, C.; Ochterski, J. W.; Ayala, P. Y.; Morokuma, K.; Voth, G. A.; Salvador, P.; Dannenberg, J. J.; Zakrzewski, V. G.; Dapprich, S.; Daniels, A. D.; Strain, M. C.; Farkas, O.; Malick, D. K.; Rabuck, A. D.; Raghavachari, K.; Foresman, J. B.; Ortiz, J. V.; Cui, Q.; Baboul, A. G.; Clifford, S.; Cioslowski, J.; Stefanov, B. B.; Liu, G.; Liashenko, A.; Piskorz, P.; Komaromi, I.; Martin, R. L.; Fox, D. J.; Keith, T.; Al-Laham, M. A.; Peng, C. Y.; Nanayakkara, A.; Challacombe, M.; Gill, P. M. W.; Johnson, B.; Chen, W.; Wong, M. W.; Gonzalez, C.; Pople, J. A. *Gaussian 03*, revision C.02; Gaussian, Inc.: Wallingford, CT, 2004.2004.